THE JOURNAL OF BIOLOGICAL CHEMISTRY VOL. 284, NO. 49, pp. 34019–34027, December 4, 2009
© 2009 by The American Society for Biochemistry and Molecular Biology, Inc. Printed in the U.S.A.

Structural Snapshots of Heparin Depolymerization by Heparin Lyase I*[S]

Received for publication, May 28, 2009, and in revised form, August 12, 2009 Published, JBC Papers in Press, October 2, 2009, DOI 10.1074/jbc.M109.025338

Young-Hyun Han[‡§1], Marie-Line Garron[¶1], Hye-Yeon Kim[‡1], Wan-Seok Kim[‖], Zhenqing Zhang[**], Kyeong-Seok Ryu[‡], David Shaya[¶], Zhongping Xiao[**], Chaejoon Cheong[‡], Yeong Shik Kim[‖], Robert J. Linhardt[**], Young Ho Jeon[‡,‡‡2], and Miroslaw Cygler[¶§§3]

From the [‡]Magnetic Resonance Team, Korea Basic Science Institute, Ochang, Chungbuk 363-883, Korea, the [¶]Department of Biochemistry, McGill University, Montréal, Québec H3A 2T5, Canada, the [‖]Natural Products Research Institute, College of Pharmacy, Seoul National University, Seoul 151-742, Korea, the [**]Departments of Chemistry and Chemical Biology, Biology and Chemical and Biological Engineering, Center for Biotechnology and Interdisciplinary Studies, Rensselaer Polytechnic Institute, Troy, New York 12180, the [§§]Biotechnology Research Institute, National Research Council, Montréal, Québec H4P 2R2, Canada, the [§]Department of Biochemistry, College of Natural Sciences, Chungbuk National University, Cheongju 361-763, Korea, and the [‡‡]Department of Bio-analytical Science, University of Science and Technology, Gwahangno 113, Yusong-gu, Taejon 305-333, Korea

Heparin lyase I (heparinase I) specifically depolymerizes heparin, cleaving the glycosidic linkage next to iduronic acid. Here, we show the crystal structures of heparinase I from *Bacteroides thetaiotaomicron* at various stages of the reaction with heparin oligosaccharides before and just after cleavage and product disaccharide. The heparinase I structure is comprised of a β-jelly-roll domain harboring a long and deep substrate binding groove and an unusual thumb-resembling extension. This thumb, decorated with many basic residues, is of particular importance in activity especially on short heparin oligosaccharides. Unexpected structural similarity of the active site to that of heparinase II with an $(\alpha/\alpha)_6$ fold is observed. Mutational studies and kinetic analysis of this enzyme provide insights into the catalytic mechanism, the substrate recognition, and processivity.

Heparin and heparan sulfate are linear, negatively charged polymers consisting of repeating units of 1→4-linked uronic acid (L-iduronic acid (IdoA)[4] and D-glucuronic acid (GlcA)) and glucosamine (1). Heparin consists of a high proportion of IdoA (~90%) and is highly sulfated. It is widely used as an anticoagulant based on its binding to antithrombin, leading to the accelerated inhibition of the blood coagulation cascade (2). Heparin interacts with a variety of proteins, such as growth factors and chemokines, suggesting its relevance in various physiological and pathological processes (2, 3).

Glycosaminoglycans in general, and heparin in particular, can be degraded by two mechanisms: hydrolysis and lytic elimination (4). Glycosaminoglycan hydrolases, present in eukaryotes and prokaryotes, break the glycosidic bond to the nonreducing end of the glucosamine, whereas glycosaminoglycan lyases, found only in prokaryotes, break the glycosidic linkage to the nonreducing end of uronic acid (5). The lyases that cleave chondroitin sulfate and hyaluronan have been extensively studied, structurally and biochemically. All of these lyases share a common fold, $(\alpha/\alpha)_5$ barrel, and antiparallel β-sheet, and have similar catalytic mechanisms (6–8). In contrast, dermatan sulfate (chondroitin B) lyase has a completely different fold as a parallel β-helix, similar to pectate lyases, and employs very different catalytic machinery (9).

The eliminative depolymerization of heparin/heparan sulfate affording unsaturated oligosaccharide products is carried out by three families of enzymes (10). Their primary sequences show no recognizable similarity, and they have distinct specificities (11). Thus, heparinase I is specific for heparin cleaving the glycosidic linkage to the nonreducing end of IdoA, heparin lyase III (heparinase III) cleaves the heparan sulfate next to glucuronic acid, and heparin lyase II (heparinase II) can depolymerize both of these substrates (see Fig. 1*A*). Structural information on the heparin degrading enzymes is limited to the *Pedobacter heparinus* (formerly *Flavobacterium heparinum*) heparinase II, which adopts an overall fold similar to chondroitin and hyaluronan lyases (12). Heparinases recently have been used to identify a contaminant in commercial heparin that caused multiple deaths (13).

To determine whether there is a structural similarity between heparinase I and other lyases and to augment our understanding of substrate specificity, catalytic mechanism, and processivity, we determined the structure of *Bacteroides thetaiotaomicron* heparinase I in a free state (two crystal forms) in a complex with heparin disaccharide product (HE_2), tetrasaccharide substrate (HE_4',cleaved by the enzyme), and a

* This work was supported, in whole or in part, by National Institutes of Health Grants GM38060 and HL62244 (to R. J. L.). This work was also supported by the Top-brand Research Program (T29220, Korea Basic Science Institute) (to Y. H. J.), the 21C Frontier Microbial Genomics and Applications Center program (to Y. H. J.), and the Canadian Institutes of Health Research Grant MOP-48370 (to M. C.).

[S] The on-line version of this article (available at http://www.jbc.org) contains supplemental methods, Figs. S1 and S2, and an additional reference.

The atomic coordinates and structure factors (codes 3IKW, 3ILR, 3IMN, 3IN9, and 3INA) have been deposited in the Protein Data Bank, Research Collaboratory for Structural Bioinformatics, Rutgers University, New Brunswick, NJ (http://www.rcsb.org/).

[1] These authors contributed equally to this work.
[2] To whom correspondence may be addressed: Korea Basic Science Institute. E-mail: yhjeon@kbsi.re.kr.
[3] To whom correspondence may be addressed. E-mail: mirek@bri.nrc.ca.

[4] The abbreviations used are: IdoA, iduronic acid; Ni-NTA, nickel-nitrilotriacetic acid; SeMet, selenomethionine.

This is an Open Access article under the CC BY license.

H151A-inactive mutant with a dodecasaccharide (HE_{12}) substrate.

EXPERIMENTAL PROCEDURES

Cloning and Site-directed Mutagenesis—A genomic DNA was isolated from the *B. thetaiotaomicron* strain WAL2926 (Korean Culture Center of Microorganisms), and the gene coding for heparinase I was obtained by PCR from genomic DNA using the forward primer 5′-AAGGATCCCTGACTGCTCAGACTAAAAATACGC-3′ and the reverse primer 5′-TTGAATTCTATTATCTTTCCGAATATC-3′. The amplified PCR products were inserted into two different vectors: the *pelB*-removed pET22b plasmid (Novagen) treated with the NdeI/XhoI restriction enzyme that resulted in heparinase I with Leu-Glu-His_6 at the C terminus and the pET15b (Novagene) derivative that contained an N-terminal His_8 tag followed by a tobacco etch virus protease cleavage site. The final plasmids were verified by DNA sequencing.

Single amino acid mutants were made using the QuikChange site-directed mutagenesis kit (Stratagene), following the manufacturer's protocol. In tip deletion (Δ191–213) and thumb deletion (Δ156–221) mutants, the deleted segment was replaced by Gly-Gly-Ser tripeptide. For the activity assay, all of the mutants and deletion mutants were prepared using Ni-NTA resin (Qiagene) as centrifugation method.

Protein Expression and Purification—The recombinant heparinase I and its mutants were expressed in *Escherichia coli* BL21(DE3) cells, and protein expression was induced by 0.2 mM isopropyl β-D-1-thiogalactopyranoside at an A_{600} of 0.6, and the incubation temperature was decreased from 37 °C (used for bacterial growth prior to induction) to 20 °C. After overnight growth, the cells were harvested by centrifugation at 2,700 × *g* for 20 min at 4 °C and stored at −20 °C in 50 mM HEPES, pH 7.0. Selenomethionine (SeMet)-labeled heparinase I was expressed in methionine auxotroph DL41(DE3) and B834(DE3) cells (Novagen) grown at 20 °C overnight.

Two different heparinase I constructs (see above) were purified in different ways. Frozen cells were resuspended in lysis buffer (50 mM HEPES, pH 7.0, 150 mM NaCl, 5 mM β-mercaptoethanol, 1% Triton X-100, 1 mM benzamidine, and 20 mM imidazole) and disrupted by intermittent sonication on ice water. The lysate was separated from debris by centrifugation at 32,500 × *g* for 45 min at 4 °C. The cleared supernatant was applied onto 3 ml of Ni-NTA beads (Qiagen) pre-equilibrated with 20 ml of lysis buffer and washed two times with 10 column volumes buffer A (50 mM HEPES, pH 7.0, 150 mM NaCl, and 5 mM β-mercaptoethanol); heparinase I was eluted with buffer A containing 300 mM imidazole, and dialyzed against buffer A. The His tag was cleaved by overnight incubation with tobacco etch virus protease at an ambient temperature (protein:tobacco etch virus molar ratio of 200:1) and removed by passing the protein trough a 1-ml Ni-NTA column. Recovered protein was loaded onto an HR 10/10 Mono S cation exchange column (Amersham Biosciences). The column was washed twice (50 mM and 125 mM NaCl, 2 column volumes), and a 125–250 mM linear NaCl gradient was applied. Heparinase I eluted at ~0.17 M NaCl. Heparinase I-containing fractions were pooled and concentrated, using a Centricon YM-100 (Millipore Corp.), to 17 mg/ml. The cell pellets were resuspended in buffer A (20 mM Tris-HCl, pH 7.5, 500 mM NaCl, and 10 mM imidazole) and lysed by sonication. The soluble crude extract was applied to a HisTrap (GE Healthcare) column, which was pre-equilibrated with buffer A and washed with 12 column volumes of buffer A. Heparinase I was eluted with buffer B (20 mM Tris-HCl, pH 7.5, 500 mM NaCl, and 60 mM imidazole). The eluant was concentrated by ultrafiltration (Millipore) and loaded on a Superdex 75 16/60 gel-filtration column (GE Healthcare) pre-equilibrated with 20 mM Bis-Tris buffer, pH 5.5, 200 mM NaCl, and 1 mM dithiothreitol. Fractions containing heparinase I were collected and concentrated to 22 mg/ml in 20 mM Bis-Tris buffer, pH 5.5, 200 mM NaCl, and 10 mM dithiothreitol using an Amicon Ultra-4 filter unit (Millipore). SeMet-labeled heparinase I was purified as described above for the wild type heparinase I.

Crystallization and Data Collection—Orthorhombic heparinase I crystals were obtained from the Qiagen Classics II suite using a sitting drop setup. Heparinase I, at 17 mg/ml, was mixed at a 1:1 ratio with the reservoir solution. Crystals appeared over reservoir containing 0.1 mM HEPES, pH 7.5, and 25% polyethylene glycol 3350 (w/v). Optimization using the hanging drop method led to the best crystals obtained from reservoir solution containing 22.5% PEG 3350, 0.1 M Tris-HCl, pH 7.0, and 0.8 mM $CaCl_2$. The crystals were cryoprotected using ethylene glycol at final concentration of 21% (v/v) and flash cooled in nitrogen stream at 100 K. For native heparinase I data extending to 1.3 Å resolution were recorded at a wavelength of 0.9800 Å using a MAR CCD 300-mm area detector at the Southeast Regional Collaborative Access Team beamline, Advanced Photon Source, Argonne National Laboratory. SeMet crystals were grown under the same conditions and were isomorphous to the native crystals. The SeMet-labeled crystals diffracted to 1.4 Å at the selenium absorption peak (λ = 0.9793 Å), and the data were recorded in the same manner as the native data. To obtain enzyme-substrate/product complex, the crystals were soaked for 5–10 min in a solution containing 21% ethylene glycol (v/v) and 5 mM heparin tetrasaccharide (2-sulfo-IdoA-β(1→4)-2,6-disulfo-GlcN)$_2$. Diffraction data extending to 1.3 Å resolution were recorded as described above.

Different crystallization conditions led to a monoclinic crystal form of heparinase I. Initial crystals were obtained using the sitting drop vapor diffusion method at 20 °C, with heparinase I concentrated to 22 mg/ml with 0.1 M citrate buffer, pH 5.5, and 2.0 M ammonium sulfate as mother liquor. These crystals were reproduced by the hanging drop vapor diffusion method and used for data collection. The crystals were soaked in cryoprotectant solution containing 20% glycerol and were flash-cooled in liquid nitrogen. SeMet-labeled heparinase I crystals were obtained under the same conditions. To obtain ligand complex structure, 10 mM disaccharide heparin (HE_2) and 6 mM dodecasaccharide heparin (HE_{12}) were incubated with the native heparinase I and heparinase I-H151A mutant, respectively. The HE_2 complex crystals were obtained in 22% glycerol, 20% PEG 1500, and 10 mM sarcosine. HE_{12} complex crystals were obtained in 10% glycerol, 8% PEG 1500, and 10 mM sarcosine. X-ray diffraction data of native and ligand complex crystals were collected using the ADSC Quantum210 CCD detector at Pohang Accelerator Laboratory beamline 4A (Pohang, Korea).

SeMet-labeled heparinase I multiwavelength anomalous dispersion method diffraction data sets were collected using a Bruker AXS Proteum300 CCD detector at Pohang Accelerator Laboratory beamline 6B (Pohang, Korea). All data sets were integrated and scaled using HKL2000 (14), with the data collection statistics summarized in Table 1.

Structure Determination and Refinement—The structure of heparinase I of orthorhombic was solved by single wavelength anomalous dispersion method (15). A total of six selenium sites were located using the program SHELXD (16). The refinement of heavy atom sites and solvent flattening were performed using SHARP (17). The initial model was built with COOT (18) and refined with REFMAC5 (19) against the single wavelength anomalous dispersion data set, and the final model was refined against the native data set extending to a higher resolution. A strong peak in the electron density was interpreted as a Ca^{2+} ion based on the ligand geometry and reasonable B-factors. Refinement at 1.3 Å resolution for native heparinase I, and 1.5 Å resolution for heparin-soaked heparinase I converged with an *R*-factor/R-free of 0.185/0.208 and 0.174/0.206, respectively, with one monomer in the asymmetric unit consisting of residues 3–376 and one bound Ca^{2+}. The native model also contained four molecules of ethylene glycol and 405 water molecules (Table 1). The heparinase I heparin soak model contained five molecules of ethylene glycol and 328 water molecules. Residue 326 is disordered in the native structure, and residues 324–329 are disordered in the above-mentioned data sets, hence they were not modeled.

The structure of the monoclinic form of heparinase I was solved by multiwavelength anomalous dispersion method using the programs Solve (20) and Resolve (21). The initial model was built with COOT (18) and refined with REFMAC5 (19). The refinement of two structures of the heparinase I-ligand complex such as HE_2 and HE_{12} were performed using REFMAC5 (19) and CNS (22). All final models were validated by PROCHECK (23). X-ray data collection and refinement statistics are given in Table 1.

Activity Assay—Heparinase activities were determined by measuring the formation of the C4–C5 double bond at the nonreducing end of heparin products indicated by the absorption at 232 nm. The reaction was performed with 2 μg of heparinase I and various lengths of heparins (from tetramer to dodecamer, and low molecular weight heparin with an average molecular weight of 5,700 as 20-mer) as substrate in a concentration range of 50–150 μM in 1 ml of reaction buffer containing 20 mM Tris-HCl, pH 7.5, 200 mM NaCl, and 10 mM $CaCl_2$. Activity of the wild type and all the described mutants were compared under the same condition. Kinetic constants of wild type heparinase I and tip deletion mutant (Δ191–213) were measured for heparin 20-mer, hexamer, and octamer. The kinetic parameters were derived from initial velocities obtained at six to seven different concentrations (10–45 μM) for wild type and five to seven concentrations (70–350 μM) for tip deletion mutant (Δ191–213) of low molecular weight heparin, hexamer, and octamer. The kinetic parameters (K_m, V_{max}, and k_{cat}) were calculated based on the Lineweaver-Burk equation (10, 24).

Isothermal Titration Calorimetry—To determine the binding affinities of heparinase I-H151A (full-length) and deletion mutants, Δ156–221 (thumb deletion) and Δ191–213-H151A (tip deletion), we performed calorimetric titrations using a VP-isothermal titration calorimeter (VP-ITC) (MicroCal) at 15 °C and processed the data with MicroCal Origin 7.0 software. The proteins and heparin oligosaccharides were individually buffer-exchanged into an identical lots of reaction buffer (25 mM Tris, pH 7.5, 200 mM NaCl, and 1 mM dithiothreitol) using dialysis overnight. Then, proteins and heparin oligosaccharides were degassed for 15 min. For titration, heparin substrates were added to the enzyme and its mutants in 30 consecutive aliquoted injections until the proteins were saturated with ligand.

RESULTS AND DISCUSSION

Three-dimensional Structures of Heparinase I and Its Complexes at Various Stages of the Reaction—The three-dimensional structures (apo, HE_{12}, HE_4', and HE_2 complexes) of heparinase I were determined at 1.4 ~ 2.0 Å resolution by x-ray crystallography (Table 1). Heparinase I is composed of a β-jellyroll domain made of two concave β-sheets (eight antiparallel β-strands each) that have a glucanase fold (SCOP database; Ref. 25) and the thumb-like insertion domain (thumb domain, residues 156–221) extending from one side of the β-jellyroll (Fig. 1*B*). A smaller extension forms an Ω loop (residues 92–118) with an embedded α-helix. The thumb domain has an unusual shape with a base formed by five short antiparallel β-strands flanked by an α-helix and extended to the side by a triangular arrangement of two long and one short strands (Fig. 1*C*). This domain represents a new fold not observed previously. The same shape and orientation of the thumb domain is seen in two crystal forms with very different packing, indicating that despite the appearance of flexibility, this domain is relatively rigid. The inner sheet of the β-jellyroll is strongly curved, forming a long extended canyon that traverses the β-strands. This canyon is highly positively charged and provides a binding site for heparin. Moreover, the thumb domain is also positively charged, predominantly on the side facing the canyon, and appears to facilitate binding of a negatively charged heparin (Fig. 2*A*). The canyon is partially covered by a "lid" formed by two loops, Gly^{74}-Glu^{79} and Thr^{250}-Asn^{257} from the β-jellyroll domain and Lys^{184}-Val^{187} from the thumb domain (Fig. 2*B*). The structural integrity of heparinase I is aided by a Ca^{2+} ion bound in the hinge region between the β-jellyroll domain and the thumb domain and coordinated by side chains from several loops. The equatorial ligands of the pentagonal bipyramid are Oε1 (2.8 Å) and Oε2 (2.6 Å) of Glu^{222}, Oδ2 (2.3 Å) of Asp^{346}, and the backbone carbonyl oxygens of Trp^{248} (2.4 Å) and Asn^{345} (2.5 Å). The axis ligands of the bipyramid are Oδ1 of Asp^{155} (2.8 Å) and a water molecule (2.6 Å) (Fig. 1*D*).

To visualize the dynamics of heparinase I during catalytic cycle, we have captured the enzyme at various stages of the reaction. The heparinase I(H151A)-HE_{12} complex shows how an extended heparin substrate binds to the enzyme within the positively charged canyon (Fig. 2*A*). The second complex shows a tetrasaccharide substrate just after cleavage of the glycosidic

TABLE 1
Data collection and refinement statistics

	Native 1		SeMet 1		HE_2 complex	HE_{12} complex	Native 2	SeMet 2	HE_4 complex
					Data Collection				
Space group	C2	C2	C2	C2	C2	C2	$P2_12_12$	$P2_12_12$	$P2_12_12$
Cell dimensions									
a, *b*, *c* (Å)	116.9,68.7, 61.3		116.6,69.0,61.0		112.8, 63.5, 65.2	112.2, 63.4, 65.3	76.2, 110.4, 44.1	76.1, 110.4, 44	75.7, 109.6, 43.8
α, β, γ (°)	90, 105.9, 90		90, 107.0, 90		90,115.47,90	90,112.39,90	90, 90, 90	90, 90, 90	90, 90, 90
		Peak	*Inflection*	*Remote*				*Peak*	
Wavelength	1.00000	0.97905	0.97924	0.97136			0.99999	0.97930	0.97929
Resolution (Å)*	50-1.8(1.8-1.86)	50-2.5	50-2.5	50-2.5	50-2.0(2.0-2.07)	50-1.9(1.90-1.97)	50-1.3(1.35-1.3)	45-1.4(1.5-1.4)	20-1.5(1.53-1.5)
R_{merge}	0.057(0.178)	0.082(0.275)	0.075(0.278)	0.079(0.305)	0.066(0.102)	0.069(0.230)	0.086(0.599)	0.052(0.47)	0.060(0.373)
I / σ(I)	37.14(4.67)	22.69(3.49)	21.97(3.41)	19.98(2.88)	28.88(11.62)	42.89(8.79)	18.2(1.75)	14.1(5.8)	28.4(2.8)
Completeness (%)	92.2(55.3)	88.8(59.3)	88.3(60.2)	86.4(55.9)	99.0(95.7)	99.8(99.5)	99(92.4)	92.3(88.6)	96.7(75.7)
Redundancy	4.4(3.2)	6.4(4.7)	6.4(4.6)	6.3(4.1)	3.8(3.4)	7.4(7.0)	4.9(3.5)	6.7(6.2)	6.7(4.1)
					Refinement				
No. reflections	38,365				28,059	32,566	86,555		54,567
R_{work} / R_{free}	0.179/0.204				0.183/0.217	0.194/0.222	0.185/0.208		0.174/0.206
No. atoms									
Protein	2,980				2,978	2,951	3,050		3,021
Ligand/ion	31(6 SO4, 1 Ca)				70/1	145/1	25(6 EDO, 1 Ca)		97 (5 EDO, 2 IDD, 2 SGN, 1 Ca)
Water	284				303	231	405		328
B-factors									
Protein	26.8				26.212	30.038	17.3		15.5
Ligand/ion	58.7				61.737/18.74	41.711/21.130	20.8		21.9
Water	33.9				35.501	36.544	29.8		25.2
R.m.s deviations									
Bonds (Å)	0.014				0.0053	0.0055	0.020		0.022
Bond angles (°)	1.45				1.504	1.547	1.95		1.98

[a] Values in parentheses are for highest resolution shell.

linkage. Finally, the third complex shows one of the products bound to the enzyme at the negative "−" subsites (26).

Dodecasaccharide Substrate—Eight sugar units of the dodecasaccharide substrate could be fitted well in electron density map, and the electron density was especially well defined for the hexasaccharide occupying subsites −2 to +4 (with cleavage taking place between the −1 and +1 sugar) (Fig. 2*B*) (26). The substrate binding involves many direct and water-mediated hydrogen bonds between the sulfate groups and the basic side chains within the canyon. The free hydroxyl groups of sugars in subsites +2, +1, and −1 are also hydrogen-bonded to the enzyme. The acidic groups at subsites +3, +1, and −2 are involved in hydrogen bonds to the side chains. Of these, the carboxylic group at +1 sugar is the most tightly bound, forming two H-bonds to the side chain of Gln^{149} and a third to the side chain of Arg^{83}. No stacking between the aromatic residues and the sugar rings is observed, which is rather unusual for the carbohydrate binding sites. Instead, Tyr^{226} is wedged perpendicularly against the hydrophobic surface of the −1 sugar ring. The β-sheet of the thumb domain participates in substrate binding in the positive "+" subsites through Lys^{185} and Gln^{223}.

To fit into the enzyme's binding site, the long polysaccharide has to adjust its conformation. First, the chain makes a tight 90° bend centered at GlcNAc in the +2 subsite (Fig. 3*A*). This bending is necessary to accommodate an extended chain and allow the +3 and +4 sugars to emerge on the protein surface. The second feature is the higher energy twist conformation assumed by the sugar ring in the −2 subsite (28). This conformation allows the −3 sugar to emerge to the protein surface at the other end of the canyon (see below), as is illustrated by the surface representation of heparinase I (Fig. 2*A*). Several oligosaccharide degrading enzymes acting either by hydrolytic (*e.g.* lysozyme) or lyase (*e.g.* chondroitinase AC and chondroitinase B) mechanisms are known to force the substrate to bind with the key sugar ring in an energetically less favorable non-chair conformation. It is thought that imposing strain on the bound substrate lowers the energy barrier of the transition state (29, 30). Heparinase I also utilizes this mechanism but for a different reason. When the enzyme binds a long polysaccharide chain in the middle (endolytic cleavage), it forces a non-chair conformation on a sugar ring in the −2 subsite that allows the remainder of the chain on the nonreducing end to reach the surface (Fig. 3*A*).

Upon binding of the long HE_{12} polysaccharide, the lid-forming loops move slightly toward the substrate, and the thumb domain rotates forward by 11° around the hinge located near Asp^{155} (Fig. 4), together creating a tighter fit as compared with other complexes. The movement of the thumb is much smaller for shorter substrates, indicating a role of the thumb domain in binding long polysaccharides. Moreover, the lid loop Glu^{73}-Thr^{80} covering the − subsites, which is partially disordered in the apo structure of the orthorhombic form, becomes well ordered in the structures of heparinase I-oligosaccharide complexes (also ordered in the apo heparinase I in the monoclinic form), suggesting that its mobility plays an important role in substrate binding and product release.

Tetrasaccharide Just after Cleavage—The structure of a cleaved tetrasaccharide bound to heparinase I shows that the breaking of the glycosidic linkage does not require significant movement of the substrate in subsites +2, +1, and −1. The sugar ring in the +1 subsite (unsaturated uronic acid, ΔUA) is now unsaturated, containing a C4–C5 double bond, and, consequently, the ring assumes a half-chair conformation (Fig. 1*A*). The distance between the C4 of ΔUA in the +1 subsite and the new O1 of GlcNAc in the −1 subsite increases from the bond length of 1.4 Å to a distance of 2.8 Å, resulting in only a small movement of these sugars with the preservation of hydrogen bonds and van der Waals contacts (Fig. 3, *A* and *B*). Interestingly, unlike in the bound dodecasaccharide, the sugar in the −2 subsite is in the energetically favorable chair conformation, and the sulfate group occupies a different side niche of the binding site as compared with the same sugar in a dodecasaccharide

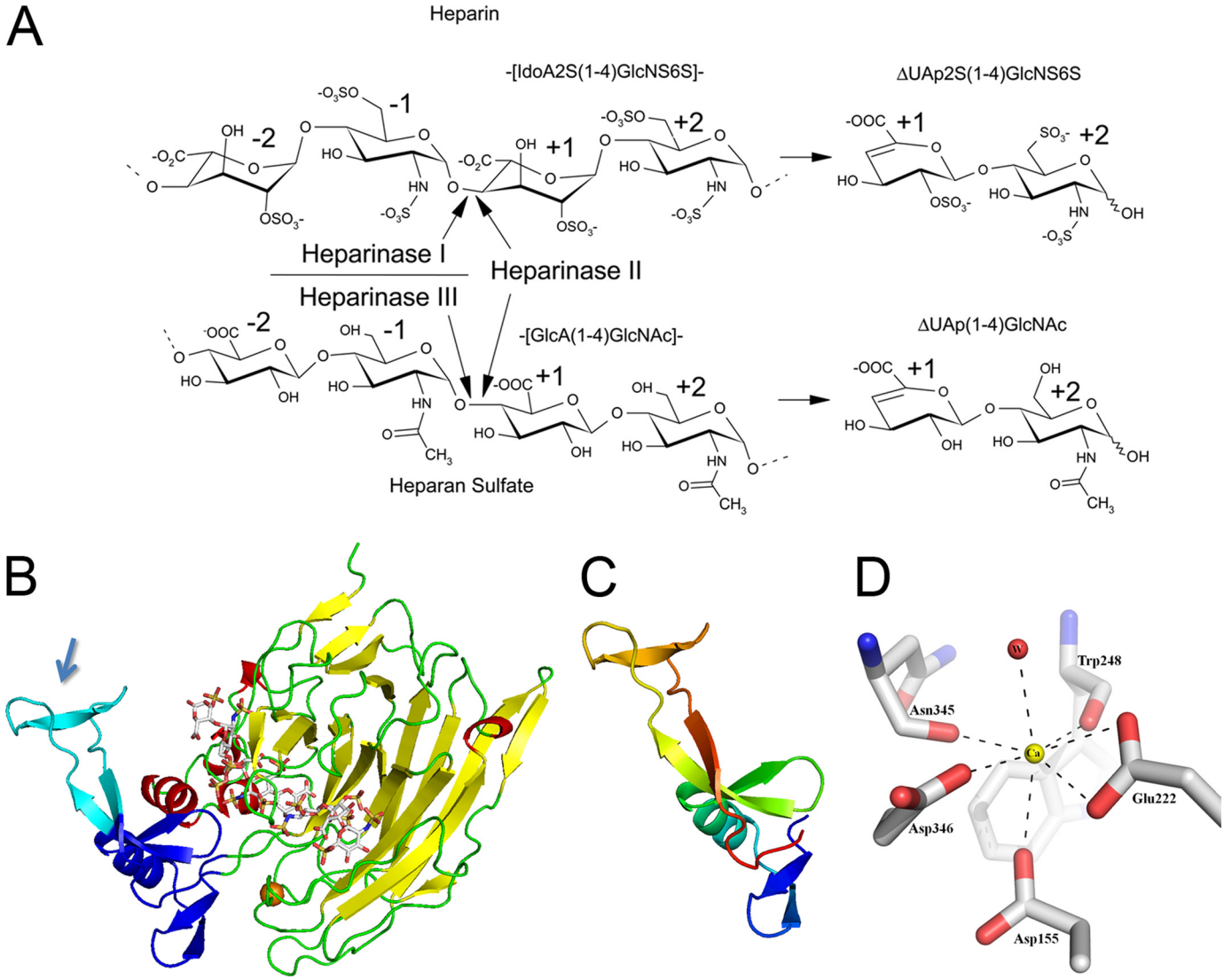

FIGURE 1. **Overall structures of heparinase I.** *A*, degradation of heparin and heparin sulfate by heparinases I–III. The naming of the sugar sites follows the nomenclature introduced by Davies *et al.* (26). The *arrows* indicate the cleavage site. *B*, schematic representation of the heparinase I-H151A-heparin oligosaccharide (HE_{12}) complex. The heparin is shown in *stick* representation, and Ca^{2+} is shown as an *orange sphere*. The thumb domain is colored *blue*, and the tip of the thumb (indicated by the *blue arrow*) is colored *cyan*. *C*, close-up of the thumb domain rainbow (*blue*, N terminus; *red*, C terminus). *D*, bipyramidal coordination of a Ca^{2+} ion in apo heparinase I structure. These and subsequent figures were prepared with PyMOL (27).

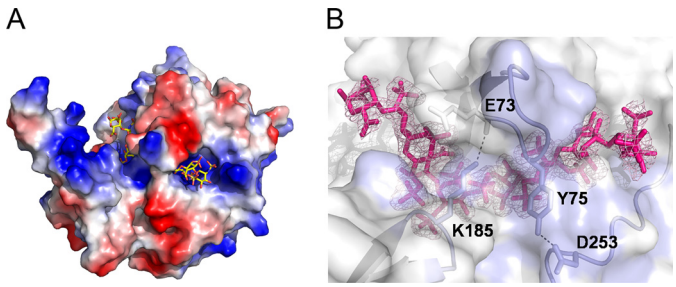

FIGURE 2. **Structures of bound heparin HE_{12} in heparinase I.** *A*, bound heparin HE_{12} in the positively charged canyon of heparinase I-H151A shown as surface charge presentation. *B*, the electron density around eight clearly visible sugar units of dodecasaccharide contoured at 1σ level. Glu^{73} and Tyr^{75} in the loop connecting β6 and β7 make a hydrogen bond with Lys^{185} and Asp^{253}, respectively.

(Fig. 3, *A* and *B*). The conformation observed in the tetrasaccharide, while energetically favored, is not compatible with a longer polysaccharide because the next sugar unit attached to the ring in this conformation would collide with the sides of the canyon. This example clearly shows that the conclusions reached from investigating shorter oligosaccharide substrates may not be fully transferable to a longer polysaccharide due to the "end effects." Moreover, the electron density for the product in + subsites is significantly weaker than for the − subsites, suggesting substantially lower occupancy of this site (see below). This observation would be in agreement with the model where, after breaking the bond, the product on the reducing end of the polysaccharide and occupying the + subsites leaves first.

Disaccharide Product—The structure of heparinase I with the product captured in the monoclinic crystal form shows two bound disaccharides (Fig. 3*B*). The first binds in the −1 and −2 subsites overlapping very well on the corresponding sugars in the other complexes. The second disaccharide is bound in the general area of +2 and +3 subsites, but in the reverse direction to that of the substrate, does not overlap well with the dode-

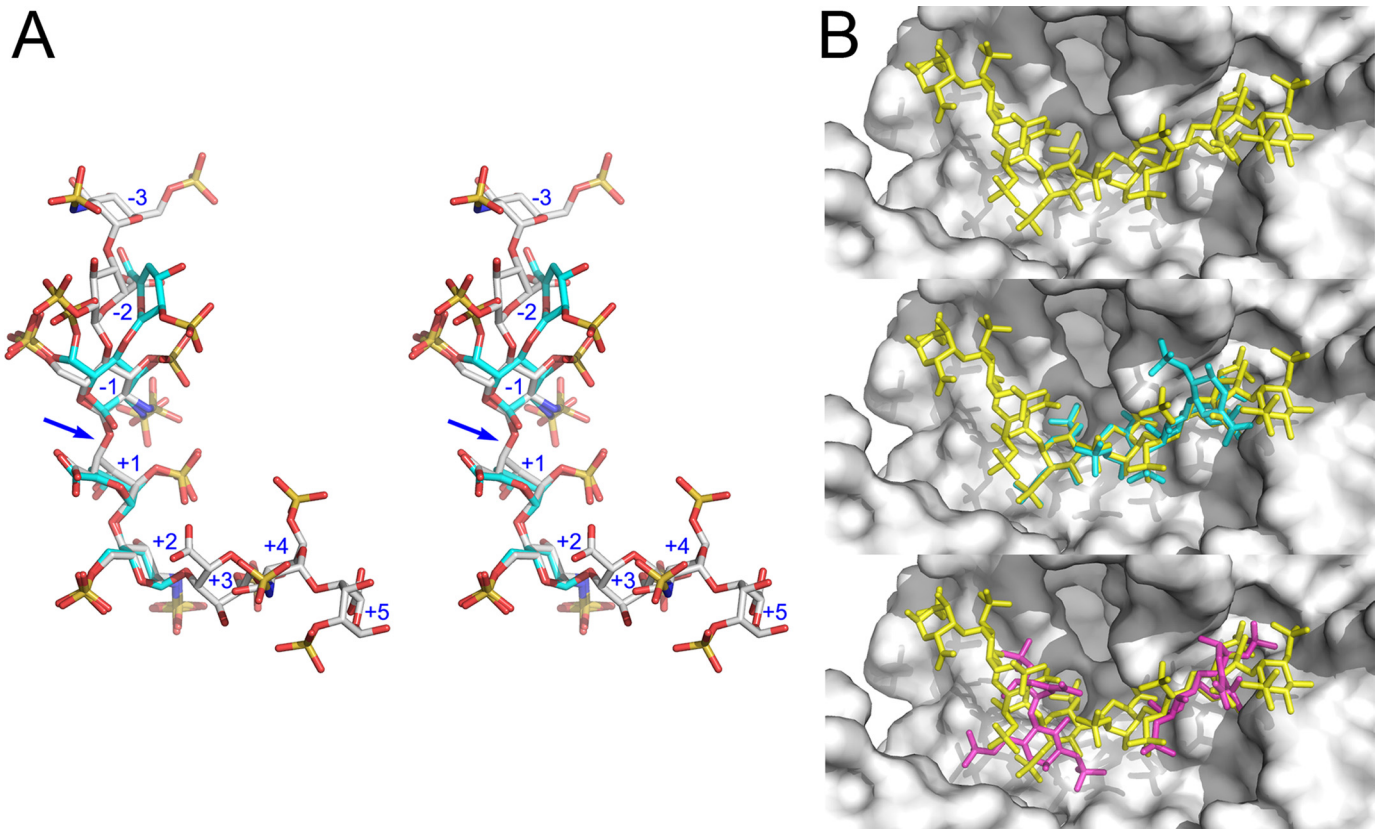

FIGURE 3. **Comparison of bound heparins.** *A*, the superposition of the tetrasaccharide (backbone carbon shown in *light blue*) and dodecasaccharide (backbone carbon shown in *white*) in the binding site. Note the 90° bend at the +2 subsite, as well as the twist conformation of the dodecamer sugar in the −2 subsite. The *arrow* indicates the cleavage site of the tetrasaccharide. *B*, comparison of the bound heparins on the molecular surface of heparinase I-H151A. The dodecasaccharide is shown in *yellow*, the tetrasaccharide is shown in *light blue*, and the disaccharide is shown in *pink*. Residues Gly^{74}-Glu^{79}, Thr^{250}-Asn^{257}, and Lys^{184}-Val^{187}, which cover the canyon, were removed for a better view of the heparin ligands.

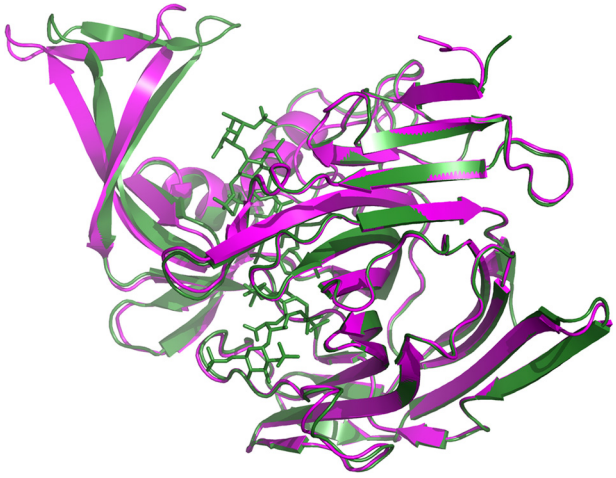

FIGURE 4. **Superposition of the heparinase I and heparinase I(H151A)-HE$_{12}$ complex.** The heparinase I(H151A)-HE$_{12}$ complex is shown in *green*, and the apo structure is shown in *magenta*. The thumb domain moves toward the dodecasaccharide substrate.

casaccharide and represent fortuitous binding to an open site. This is another indirect indication that the binding to the − subsites is stronger, with the product occupying the + subsites leaving first.

Catalytic Properties of Heparinase I—To determine whether the enzyme has a preference for the length of the polysaccharide substrate, we performed enzymatic assays and kinetic analysis of heparinase I with various length of heparin polysaccharides. The enzyme requires a minimum of six sugar units for efficient catalysis and has an overall preference for longer polysaccharides (data not shown). The kinetic data show that the k_{cat}/K_m for the 20-mer substrate is ~4.5 times higher than that of the hexasaccharide. The longer polysaccharide shows lower k_{cat}, but this is compensated by a 12-fold lower K_m (Table 2). The effect on binding was confirmed by isothermal calorimetry, which showed that the K_d of heparinase I(H151A) for heparin 20-mer is also ~12-fold lower than for the hexasaccharide (Fig. 5, *B* and *C*). Interestingly, for both the wild type and tip deletion mutant (Δ191–213), the k_{cat} for the hexameric substrate is ~3-fold higher than that of the 20-mer substrate. We rationalize that this is related to a slightly better positioning of the sugars of the hexasaccharide in the active site due to smaller steric effects (see above). The action pattern of heparinase I on a long polymeric substrate investigated using polyacrylamide gel electrophoresis and liquid chromatography-mass spectroscopy shows an endolytic pattern with a processive bias (data not shown).

Thumb Domain—The unusual shape of the thumb domain extending from the main body of the enzyme prompted us to investigate whether this domain is important for heparinase activity and substrate binding (see supplemental Fig. S1). To this end, we have constructed a deletion mutant, Δ156–221 (thumb deletion) (Fig. 1*B*). The mutant is well folded and

TABLE 2

Kinetic constants of wild type heparinase I and tip deletion mutant (Δ191–213) measured with heparin 20-mer, hexamer, and octamer. Values were derived from a molar absorbance coefficient at 232 nm for the unsaturated C4=C5 double bond of urinate of 3,800 M^{-1} cm^{-1}.

Protein	Heparin	K_m [a]	V_{max} [a,b]	k_{cat}	k_{cat}/K_m [c]
		μM		s^{-1}	
WT	20-mer[d]	4.6 ± 1.0	40.6 ± 1.4	29.1 ± 1.0	6,311
WT	Octamer	18.2 ± 2.0	101.4 ± 4.7	73.7 ± 3.4	4,054
WT	Hexamer	54.1 ± 5.7	107.8 ± 7.2	78.4 ± 5.2	1,448
Δ191–213	20-mer	239.5 ± 45.5	5.8 ± 0.8	4.0 ± 0.5	16.5
Δ191–213	Hexamer	5015.4 ± 382.9	21.1 ± 1.3	14.5 ± 0.9	3.0

[a] Values of the K_m and V_{max} are derived from initial velocities obtained at six to seven concentrations (10–45 μM) for wild type and five to seven concentrations (70–350 μM) for Δtip of low molecular mass heparin, hexamer, and octamer.
[b] V_{max} is expressed as μmol/min[chemp]mg protein.
[c] k_{cat}/K_m is expressed as mM^{-1} s^{-1}.
[d] An average molecular mass of 5,700 Da was used for substrate to calculate its molar concentration.

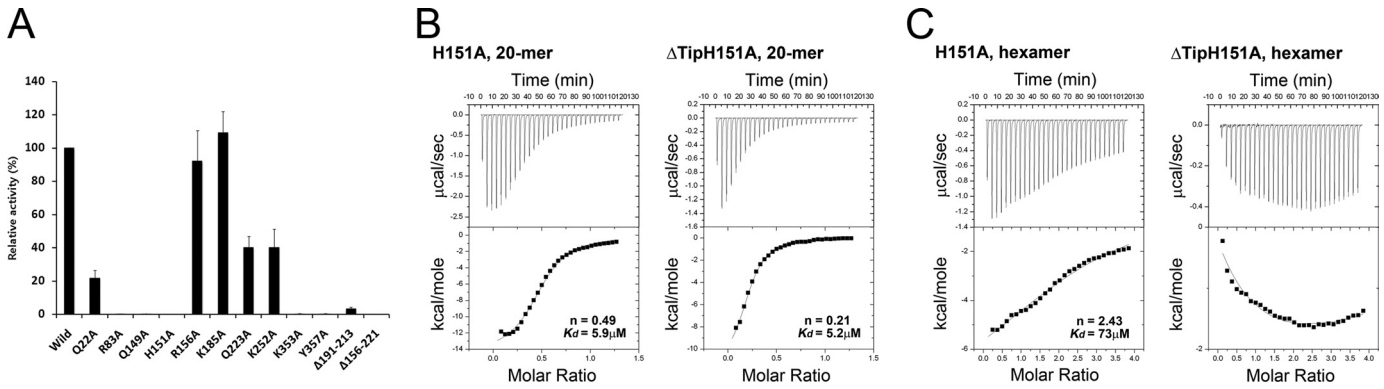

FIGURE 5. **Characterization of heparinase I mutants.** *A*, relative activities of single amino acid mutants, the thumb deletion, and the tip deletion mutant. *Error bars* show S.D. *B*, isothermal calorimetric titration of heparinase I-H151A mutant and the tip deletion-H151A upon the addition of heparin 20-mer. *C*, isothermal calorimetric titration of heparinase I-H151A mutant and the tip deletion-H151A upon the addition of heparin hexamer.

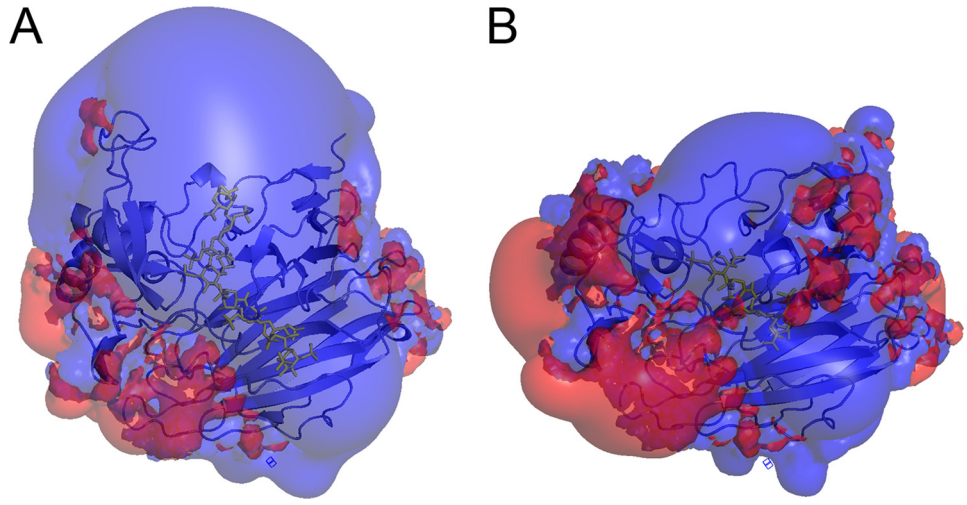

FIGURE 6. **The electrostatic potential surface.** *A*, the electrostatic potential surrounding the wild type heparinase I. Positive potential is colored *blue*, and negative potential is colored *red*. The schematic representation of heparinase I is shown together with a bound dodecasaccharide (not included in the electrostatic calculations). *B*, the potential for the tip deletion mutant. The electrostatic surfaces were calculated with program APBS (31) and contoured at 2kT (1.2 kCal/mol = 0.052 eV) level (shown as semitransparent).

retains the secondary and tertiary structure as verified by CD (data not shown) and NMR spectroscopy (supplemental Fig. S2). However, the thumb deletion mutant has lost its Ca^{2+} ion (analyzed by inductively coupled plasma mass spectrometer (ICP-MS), data not shown) and showed no detectable degradation of heparin (Fig. 5*A*). Isothermal calorimetry experiments showed that this results from the loss of its ability to bind heparin oligosaccharides and confirmed the role of the Ca^{2+} ion in organizing the residues that participate in substrate binding.

Tip of the Thumb—Next, we have constructed a smaller deletion Δ191–213 (tip deletion), where only the triangular tip of the thumb domain was removed, which we argued should not affect Ca^{2+} binding (Fig. 1*B*). Indeed, this tip deletion mutant retained the Ca^{2+} ion (analyzed by ICP-MS) and bound long heparin polysaccharide with a K_d indistinguishable from the wild type enzyme (Fig. 5*B*). However, binding of a heparin hexasaccharide to this tip deletion mutant is significantly impaired (Fig. 5*C*). Kinetic analysis shows that the catalytic efficiency of this mutant is substantially worse than the wild type enzyme. The tip deletion mutant was ~380-fold less active on heparin 20-mer than the wild type enzyme and as much as ~480-fold less active on the hexasaccharide substrate (k_{cat}/K_m, Table 2). These results demonstrate the crucial role of the tip region for enzyme activity.

To explain this essential role of the thumb that is relatively distant from the active site, we calculated the electrostatic potential of heparinase I and of the tip deletion mutant. The striking feature of wild type heparinase I is a strong positive electrostatic field extending over the entry to the binding site

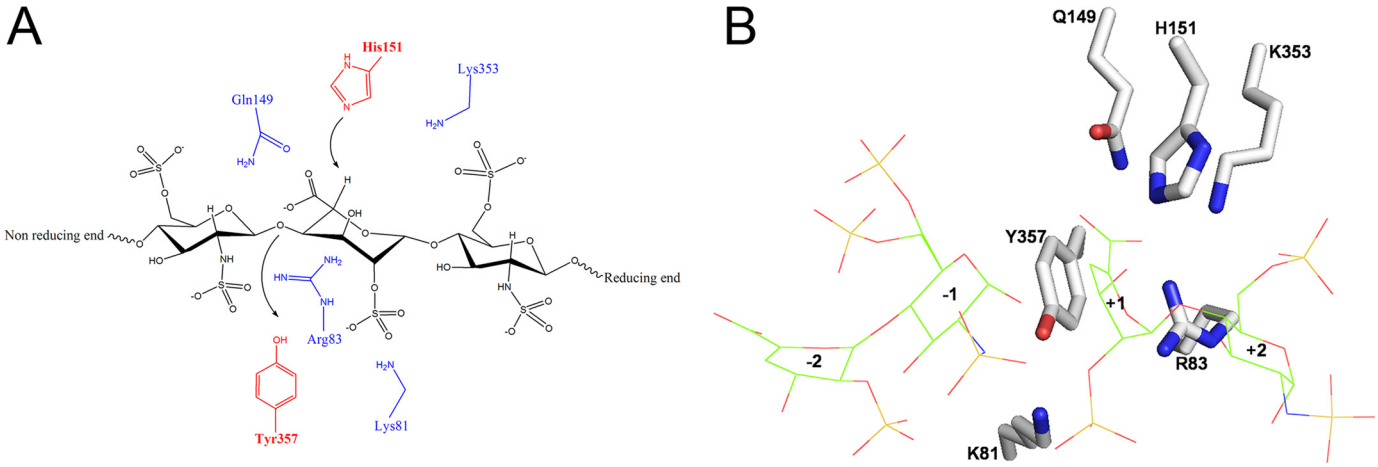

FIGURE 7. **Schematic catalytic mechanism of heparinase I.** *A*, heparinase I catalyzes the β-elimination of glycosidic linkage between the -1 and $+1$ positions of heparin substrate. His^{151} abstracts the C5 proton from L-iduronic acid in the $+1$ site, and Tyr^{357} acts as a general acid to donate a proton at the reducing end of glucosamine in the -1 subsite. The nearby Lys^{81} modulates pK_a of the Tyr^{357} hydroxyl. Gln^{149} neutralizes the carboxyl group of IdoA at subsite $+1$. *B*, shown is a close-up view of the catalytic site of heparinase I with the tetrasaccharide just after cleavage.

(Fig. 6*A*). This suggests that the electrostatic field significantly contributes to the affinity of the negatively charged substrate. Deletion of the tip dramatically decreases the electrostatic field (Fig. 6*B*), and we propose that the decrease of both K_d and K_m for short oligosaccharide substrates (hexasaccharide) results from the loss of this positive electrostatic field.

Proposed Model for Catalysis—Ten site-directed mutants (Q22A, R83A, Q149A, H151A, R156A, K185A, Q223A, K252A, K353A, and Y357A) in contact with the central segment of the dodecasaccharide were examined for their heparin-degrading activity to clarify their roles in catalysis (Fig. 5*A*). Of these, five mutants (R83A, Q149A, H151A, K353A, and Y357A) lost completely the ability to degrade heparin. Combining the structural and mutational data, we propose the following events leading to catalysis (Fig. 7*A*). The neutralization of the carboxylate group of IdoA at the $+1$ subsite is accomplished by its interaction with Gln^{149} and Arg^{83} (32). The two hydrogen bonds that are formed with Gln^{149} suggest neutralization of the negative charge on the carboxylate (C6 position) of the IdoA by Gln^{149}, which may result in resonance stabilization of the enolate form lowering the pK_a of the C5-bound hydrogen (32, 33). Lys^{353} also makes a charge interaction to the sulfate of GlcNAc in the $+2$ subsite and an additional interaction to the carboxylate group of ΔUA in the $+1$ subsite in the HE$_4$′ complex structure (Fig. 7*B*). The role of the general base, abstracting the C5 proton, is played by His^{151} (32). The histidine side chain faces the C5 proton of IdoA in the $+1$ subsite and its Nϵ2 atom is $\sim$3.0 Å away from the C5, collinear with the C5–H-bond ($\sim$2 Å from the proton). Proton abstraction leads to a β-elimination of the 1$\rightarrow$4 glycosidic linkage with the concomitant formation of a C4–C5 double bond in the ΔUA at the nonreducing end (34). Finally, the hydroxyl group of the Tyr^{357} makes a hydrogen bond to the oxygen in the glycosidic linkage in HE$_{12}$ complex structure and the C1 hydroxyl group of the -1 subsite GlcNAc in the HE$_4$′, complex structure, respectively. Tyr^{357} assumes the role of a general acid donating a proton to the O$^-$ leaving group of a glucosamine and reconstituting the hydroxyl group at the reducing end (32, 33). For Tyr^{357} to function as a general acid to donate a proton, its pK_a must lowered by the local environment. We postulate that

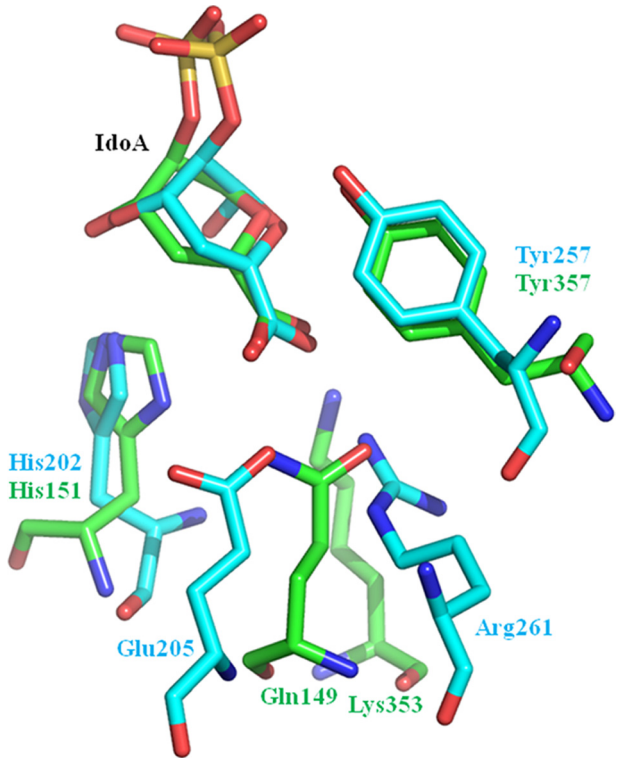

FIGURE 8. **Superposition of the active site of heparinases I and II.** Heparinase I is shown in *green*, and heparinase II is shown in *cyan* (Protein Data Bank code 2FUT). The Tyr and His residues and the IdoA in the $+1$ site superimpose very well. The carboxylic group of IdoA is stabilized by Gln and Lys in heparinase I and by Glu and Arg in heparinase II.

Lys^{81}, which makes a hydrogen bond to Tyr^{357}, reduces the pK_a of the tyrosine (35).

Convergence of Catalytic Machinery of Heparinases I and II—Despite the lack of detectable sequence similarity between heparinase I and alginate lyases belonging to two distinct sequence families, PL-13 and PL-7 (CAZy database; 36), they share a similar fold and utilize a similar catalytic mechanism (37). However, the structure of heparinase I contains several long insertions as compared with the more compact structures of alginate lyases (37), including the thumb domain, a

30-residue long N-terminal insertion, and the Ala^{91}-Gly^{117} Ω loop.

Like heparinase I, heparinase II is able to depolymerize heparin. The structure of *P. heparinus* heparinase II recently has been determined (12). Its overall architecture is very different from that of heparinase I, with the catalytic domain being an $(\alpha/\alpha)_5$-incomplete toroid, topologically very similar to chondroitin sulfate and hyaluronan lyases and sharing with them the main features of the catalytic site. A completely different fold of heparinases I and II led to the expectation of rather different active site constellations. However, a close comparison of these two enzymes uncovers striking similarities in the arrangement of their catalytic residues (Fig. 8) strongly supporting the proposed catalytic roles for residues in both catalytic schemes. The superposition of active site residues based on the positions of the bound ΔUA sugars in +1 subsite places the catalytic His^{151} and Tyr^{357} of heparinase I onto the putative catalytic residues of heparinase II, His^{202} and Tyr^{257}. The acidic group of the ΔUA forms hydrogen bonds to Gln^{149} and Lys^{353} in heparinase I and to Glu^{205} and Arg^{261} in heparinase II. The proposed roles of these residues were supported by the mutation study (Fig. 5*A*). Therefore, these two structures represent a clear example of the convergence of two folds toward the same catalytic site and very similar enzymatic mechanism.

In conclusion, we have determined the structure of heparinase I with its ligands at various stages of the reaction demonstrating the three-dimensional structural snapshots of heparin depolymerization. Together with the mutational study and kinetic analysis of this enzyme, our investigation provides insights into the catalytic mechanism and insight into substrate recognition and processivity. We have also showed that, in contrast to a short tetrasaccharide substrate, binding of a longer oligosaccharide substrate to heparinase I is associated with a chair-to-twist conformational switch of the sugar in the −2 subsite.

Acknowledgments—We acknowledge the use of beamlines 6B and 4A at Pohang Accelerator Laboratory (PAL) and SGX CAT at the Advanced Photon Source. Use of the Advanced Photon Source was supported by the U.S. Dept. of Energy, Office of Science, Office of Basic Energy Sciences, under Contract DE-AC02-06CH11357. Use of the SGX Collaborative Access Team beamline facilities at sector 31 of the Advanced Photon Source was provided by SGX Pharmaceuticals, Inc. We also thank K. J. Kim, G. H. Kim, and H. S. Lee at PAL for assistance with x-ray data collection and thank Y. Kim and M. H. Kim at Korea Research Institute of Bioscience & Biotechnology for assistance with isothermal titration calorimetry experiments.

REFERENCES

1. Casu, B. (1985) *Adv. Carbohydr. Chem. Biochem.* **43,** 51–134
2. Capila, I., and Linhardt, R. J. (2002) *Angew. Chem. Int. Ed.* **41,** 390–412
3. Imberty, A., Lortat-Jacob, H., and Pérez, S. (2007) *Carbohydr. Res.* **342,** 430–439
4. Ernst, S., Langer, R., Cooney, C. L., and Sasisekharan, R. (1995) *Crit. Rev. Biochem. Mol. Biol.* **30,** 387–444
5. Gacesa, P. (1987) *FEBS Lett.* **212,** 199–202
6. Linhardt, R. J., Avci, F. Y., Toida, T., Kim, Y. S., and Cygler, M. (2006) *Adv. Pharmacol.* **53,** 187–215
7. Rigden, D. J., Littlejohn, J. E., Joshi, H. V., de Groot, B. L., and Jedrzejas, M. J. (2006) *J. Mol. Biol.* **358,** 1165–1178
8. Yip, V. L., and Withers, S. G. (2006) *Curr. Opin. Chem. Biol.* **10,** 147–155
9. Michel, G., Pojasek, K., Li, Y., Sulea, T., Linhardt, R. J., Raman, R., Prabhakar, V., Sasisekharan, R., and Cygler, M. (2004) *J. Biol. Chem.* **279,** 32882–32896
10. Lohse, D. L., and Linhardt, R. J. (1992) *J. Biol. Chem.* **267,** 24347–24355
11. Godavarti, R., and Sasisekharan, R. (1996) *Biochem. Biophys. Res. Commun.* **229,** 770–777
12. Shaya, D., Tocilj, A., Li, Y., Myette, J., Venkataraman, G., Sasisekharan, R., and Cygler, M. (2006) *J. Biol. Chem.* **281,** 15525–15535
13. Guerrini, M., Beccati, D., Shriver, Z., Naggi, A., Viswanathan, K., Bisio, A., Capila, I., Lansing, J. C., Guglieri, S., Fraser, B., Al-Hakim, A., Gunay, N. S., Zhang, Z., Robinson, L., Buhse, L., Nasr, M., Woodcock, J., Langer, R., Venkataraman, G., Linhardt, R. J., Casu, B., Torri, G., and Sasisekharan, R. (2008) *Nat. Biotechnol.* **26,** 669–775
14. Otwinowski, Z., and Minor, W. (1997) *Methods Enzymol.* **276,** 307–326
15. Rice, L. M., Earnest, T. N., and Brünger, A. T. (2000) *Acta Crystallogr. Sect. D Biol. Crystallogr.* **56,** 1413–1420
16. Schneider, T. R., and Sheldrick, G. M. (2002) *Acta Crystallogr. Sect. D Biol. Crystallogr.* **58,** 1772–1779
17. Bricogne, G., Vonrhein, C., Flensburg, C., Schiltz, M., and Paciorek, W. (2003) *Acta Crystallogr. Sect. D Biol. Crystallogr.* **59,** 2023–2030
18. Emsley, P., and Cowtan, K. (2004) *Acta Crystallogr. Sect. D Biol. Crystallogr.* **60,** 2126–2132
19. Murshudov, G. N., Vagin, A. A., and Dodson, E. J. (1997) *Acta Crystallogr. Sect. D Biol. Crystallogr.* **53,** 240–255
20. Terwilliger, T. C., and Berendzen, J. (1999) *Acta Crystallogr. Sect. D Biol. Crystallogr.* **55,** 849–861
21. Terwilliger, T. C. (2001) *Acta Crystallogr. Sect. D Biol. Crystallogr.* **57,** 1763–1775
22. Brünger, A. T., Adams, P. D., Clore, G. M., DeLano, W. L., Gros, P., Grosse-Kunstleve, R. W., Jiang, J. S., Kuszewski, J., Nilges, M., Pannu, N. S., Read, R. J., Rice, L. M., Simonson, T., and Warren, G. L. (1998) *Acta Crystallogr. Sect. D Biol. Crystallogr.* **54,** 905–921
23. Laskowski, R. A., MacArthur, M. W., Moss, D. S., and Thronton, J. M. (1993) *J. Appl. Crystallogr.* **26,** 283–291
24. Yang, V. C., Linhardt, R. J., Bernstein, H., Cooney, C. L., and Langer, R. (1985) *J. Biol. Chem.* **260,** 1849–1857
25. Andreeva, A., Howorth, D., Brenner, S. E., Hubbard, T. J., Chothia, C., and Murzin, A. G. (2004) *Nucleic Acids Res.* **32,** D226–D229
26. Davies, G. J., Wilson, K. S., and Henrissat, B. (1997) *Biochem. J.* **321,** 557–559
27. Delano, W. L. (2004) *The PyMOL Molecular Graphics System*, DeLano Scientific LLC, San Carlos, CA
28. Money, V. A., Smith, N. L., Scaffidi, A., Stick, R. V., Gilbert, H. J., and Davies, G. J. (2006) *Angew. Chem. Int. Ed.* **45,** 5136–5140
29. Kuroki, R., Weaver, L. H., and Matthews, B. W. (1993) *Science* **262,** 2030–2033
30. Strynadka, N. C., and James, M. N. (1996) *EXS* **75,** 185–222
31. Baker, N. A., Sept, D., Joseph, S., Holst, M. J., and McCammon, J. A. (2001) *Proc. Natl. Acad. Sci. U.S.A.* **98,** 10037–10041
32. Ogura, K., Yamasaki, M., Mikami, B., Hashimoto, W., and Murata, K. (2008) *J. Mol. Biol.* **380,** 373–385
33. Li, S., Kelly, S. J., Lamani, E., Ferraroni, M., and Jedrzejas, M. J. (2000) *EMBO J.* **19,** 1228–1240
34. Gerlt, J. A., and Gassman, P. G. (1992) *J. Am. Chem. Soc.* **114,** 5928–5934
35. Kato-Toma, Y., Iwashita, T., Masuda, K., Oyama, Y., and Ishiguro, M. (2003) *Biochem. J.* **371,** 175–181
36. Cantarel, B. L., Coutinho, P. M., Rancurel, C., Bernard, T., Lombard, V., and Henrissat, B. (2009) *Nucleic Acids Res.* **37,** D233–D238
37. Yamasaki, M., Ogura, K., Hashimoto, W., Mikami, B., and Murata, K. (2005) *J. Mol. Biol.* **352,** 11–21